**Ecological & Sustainable Materials Connect**
ISSN: 3136-344X
2026, Article ID. 2026.0003, Cite as: https://doi.org/10.69709/ESM.2026.109909

SCIFINITI PUBLISHING

Research Article

OPEN ACCESS

# Synthesis, Characterization, Applications and Computational Studies of $CA_4$ Hydrogels Incorporated with ZnO Nanoparticles [$CA_4$-ZnO]

**Princy Sowmya Ruben**[✉,1] **Nikila Sambandan**[✉,1] **Harini Selvam**[✉,1] **Kubaib Attar**[✉,2] **Imran Predhanekar**[✉,2] **Guhanathan Selvam**[✉,1,*]

[1] Department of Chemistry, Muthurangam Government Arts College (Autonomous), (Affiliated to Thiruvalluvar University, Serkadu, Vellore-632 115), Vellore-632002, Tamil Nadu, India

[2] Department of Chemistry, Islamiah College (Autonomous), Vaniyambadi 653 752, Tamil Nadu, India (Affiliated to Thiruvalluvar University, Serkadu, Vellore-632 115), Tamil Nadu, India

**Article History**

Received: January 22, 2026 Accepted: June 26, 2026 Published: July 31, 2026

**Abstract**

In this study, hydrogels ($CA_4$) were synthesized through an esterification reaction using 2-furoic acid (FA), triethanolamine (TEA), and citric acid (CA), followed by the incorporation of nano-ZnO particles to obtain $CA_4$-ZnO hydrogels. The synthesized $CA_4$-ZnO nanocomposite hydrogels were characterized using ultraviolet spectroscopy (UV), fourier transform infrared spectroscopy (FT IR), $^{1}$proton nuclear magnetic resonance spectroscopy (H NMR), $^{13}$carbon-13 nuclear magnetic resonance spectroscopy (C NMR), TGA, and SEM-EDX techniques. The results confirmed the successful incorporation of ZnO nanoparticles into the $CA_4$ network. The swelling behavior of the hydrogels was systematically investigated over a pH range of 2.0–11.0. The results demonstrated that the hydrogels exhibited the highest swelling percentage in a neutral medium (pH 7.0) compared with those in acidic and alkaline media. The equilibrium swelling increased significantly with increasing nano-ZnO concentration. Thermogravimetric analysis (TGA) showed that the $CA_4$-ZnO nanocomposite hydrogels were thermally stable up to 300 °C. Antibacterial studies against Gram-positive bacteria, including Staphylococcus aureus and Bacillus subtilis, as well as Gram-negative bacteria, namely Klebsiella pneumoniae and Escherichia coli, demonstrated excellent inhibitory activity. The antifungal study showed a lower inhibition zone. The cytotoxicity study indicated a high percentage of cell viability, while the antioxidant analysis demonstrated significant radical-scavenging activity. Molecular docking studies of the optimized hydrogels revealed that the biological activity was enhanced through the incorporation of nano-ZnO into the hydrogel matrix. [$CA_4$-ZnO] nanocomposite hydrogels showed stronger and more favorable binding to Clumping Factor A. The [$CA_4$-ZnO] nanocomposite hydrogels have the potential to overcome drug resistance and exhibit antibacterial and wound-healing properties. Thus, the hydrogels investigated in the present study may be beneficial for tissue engineering, wound healing, and other high-performance applications.

**Keywords:**

nanocomposite hydrogels; swelling behavior; antibacterial studies; antioxidant analysis; molecular docking; Clumping Factor A

## 1. Introduction

Hydrogels are polymeric networks capable of absorbing and retaining large amounts of water. These polymeric materials can swell and store a substantial volume of water within their structure while remaining insoluble in aqueous media. Due to their high-water content, hydrogels exhibit a high degree of flexibility, closely resembling natural tissues. Hydrogels absorb water due to the presence of hydrophilic groups within the polymer backbone [1]. Hydrogels are characterized by their ability to swell within

* **Corresponding Author:**
Guhanathan Selvam, Department of Chemistry, Muthurangam Government Arts College (Autonomous), (Affiliated to Thiruvalluvar University, Serkadu, Vellore-632 115), Vellore-632002, Tamil Nadu, India,
profguhanathan12@gmail.com

© 2026 Copyright by the Authors.
Licensed as an open access article using a CC BY 4.0 license.

the polymeric network. However, polymer–water interaction forces are the primary factor responsible for hydrogel swelling. Polymer–water interactions, electrostatic forces, and osmotic pressure play important roles in the swelling and expansion of the hydrogel polymeric network. Hydrogels can be categorized as non-ionic, ionic (anionic, cationic, and amphoteric), and hydrophilic hydrogels containing hydrophobic groups based on their swelling behavior. Non-ionic hydrogels, such as poly (N-vinyl pyrrolidone) and poly(ethylene oxide), swell in aqueous media due to polymer–water interactions. Hydrogels exhibit good transparency and can be easily modified. They are environmentally friendly and possess self-healing properties [2], enabling the timely delivery of drugs or nutrients [3].

Hydrogels have the ability to respond to changes in pH, temperature, metabolite concentration, and other environmental stimuli [4,5]. Chemical cross-linking enhances the mechanical strength of hydrogels [6]. This approach is highly effective for the formation of in situ hydrogel structures. Physical cross-linking techniques involve ionic interactions, as well as temperature-dependent and pH-dependent cross-linking mechanisms [7]. The wide range of applications includes tissue engineering and the design of biological tissues in both in vitro and in vivo systems [8,9], effective wound therapy [10], drug delivery [11], gene therapy [12], and the repair of blood vessels, skin, heart valves, cartilage, and tendons [13]. Additional applications include contact lens manufacturing [14], biosensors, and wastewater remediation techniques [15]. Zinc oxide (ZnO) nanoparticles have attracted considerable attention in biomedical applications due to their excellent antibacterial activity, biocompatibility, and stability. ZnO nanoparticles effectively inhibit the growth of a broad spectrum of microorganisms through the generation of reactive oxygen species and disruption of bacterial cell membranes. In addition to their antimicrobial properties, ZnO nanoparticles also promote wound healing by enhancing cell proliferation and tissue regeneration. Several metal and metal oxide nanoparticles, such as silver oxide ($Ag_2O$) [16], gold (Au), copper oxide (CuO) [17], titanium dioxide ($TiO_2$), magnesium oxide (MgO), and zinc oxide (ZnO) [18], have been extensively investigated for antibacterial and wound-healing applications due to their strong antimicrobial activity and ability to accelerate the healing process. Therefore, ZnO nanoparticles were incorporated into the $CA_4$ matrix to prepare the $CA_4$-ZnO nanocomposite, with the aim of enhancing its antibacterial activity and wound-healing potential.

Biopolymeric three-dimensional hydrogel networks are formed from biocompatible components that can absorb and retain large quantities of water while maintaining their structural integrity. Owing to their biocompatibility, biodegradability, and tunable physicochemical properties, these hydrogels have gained significant attention in biomedical applications. In the present study, the hydrogel network was developed using citric acid, triethanolamine, and 2-furoic acid as functional building components. Citric acid acts as an effective cross-linking agent due to the presence of multiple carboxyl groups, which facilitate the formation of a stable polymeric network through esterification and hydrogen-bonding interactions. Triethanolamine contributes to the stabilization of the hydrogel structure through intermolecular interactions, while 2-furoic acid introduces additional functional groups that enhance the hydrogel's physicochemical properties.

To further enhance the functional performance of the hydrogel, zinc oxide (ZnO) nanoparticles were incorporated into the polymeric matrix to form a $CA_4$-ZnO nanocomposite. The incorporation of ZnO nanoparticles into the hydrogel network enhances antimicrobial activity and promotes tissue regeneration, making the nanocomposite suitable for biomedical applications.

# 2. Experimental

## 2.1. Methods

### 2.1.1. Stage I: Synthesis of Pre-Polymers

Citric acid (CA) was used as the monomer. A quantity of 0.025 mol (4.803 g) of citric acid (CA) was dissolved in 5 mL of ethanol and then transferred into a round-bottom flask fitted with a mechanical stirrer until the monomer was completely dissolved in the ethanol.

Triethanolamine (TEA) [0.025 mol (3.3006 g)], dissolved in 5 mL of ethanol, was added dropwise to the citric acid solution using a dropping funnel. The reaction mixture was stirred at 140 °C for 1 h. The formation of a sticky white gel indicated the formation of the citric acid–triethanolamine (CT) prepolymer).

### 2.1.2. Stage II: Synthesis of Bio-Polymeric Hydrogels

2-Furoic acid (FA) [0.025 mol (2.802 g)] was dissolved in 5 mL of ethanol, added to the CT prepolymer, and stirred continuously with a mechanical stirrer at 140 °C for 2 h. The formation of a glassy brown gel of citric acid–triethanolamine–2-furoic acid (CTF) confirmed the synthesis of the parent hydrogel. The resultant gel was immersed in pure ethanol for 24 h to remove unreacted monomers and subsequently dried in a vacuum oven at 35 °C for 24 h. A similar procedure was followed by altering the chemical composition of the monomers. Table 1

2026, Vol. 1, Article ID. 2026.0003
https://doi.org/10.69709/ESM.2026.109909

lists the experimental details of the synthesized biopolymeric hydrogels. Among the different hydrogel series, $CA_4$ was selected for further investigation based on its superior swelling behavior compared with the other synthesized hydrogels.

**Table 1:** Formulation of CA-TEA-FA in distinct composition of the synthesized biopolymeric hydrogels.

| S. No | Samples | Monomer Composition (mole) | | | Description of Hydrogels |
|---|---|---|---|---|---|
| | | CA | TEA | FA | |
| 1 | CTF | 0.025 | 0.025 | 0.025 | Transparent in nature-Brown glassy gel-Insoluble in water |
| 2 | $FA_1$ | 0.025 | 0.025 | 0.01 | |
| 3 | $FA_2$ | 0.025 | 0.025 | 0.02 | |
| 4 | $FA_3$ | 0.025 | 0.025 | 0.03 | |
| 5 | $FA_4$ | 0.025 | 0.025 | 0.04 | |
| 6 | $TEA_1$ | 0.025 | 0.01 | 0.025 | |
| 7 | $TEA_2$ | 0.025 | 0.02 | 0.025 | |
| 8 | $TEA_3$ | 0.025 | 0.03 | 0.025 | |
| 9 | $TEA_4$ | 0.025 | 0.04 | 0.025 | |
| 10 | $CA_1$ | 0.01 | 0.025 | 0.025 | |
| 11 | $CA_2$ | 0.02 | 0.025 | 0.025 | |
| 12 | $CA_3$ | 0.03 | 0.025 | 0.025 | |
| 13 | $CA_4$ | 0.04 | 0.025 | 0.025 | |

### 2.1.3. Incorporation of Zinc oxide (ZnO) Nanoparticles in CA4 Biopolymeric Hydrogels

A total of 0.5 wt% zinc oxide (ZnO) nanoparticles with a particle size of less than 100 nm were incorporated into the $CA_4$ biopolymeric hydrogel matrix and stirred continuously at 35 °C for 1 h, resulting in the formation of biopolymeric nanocomposite hydrogels [$CA_4$-ZnO]. Similarly, 1.0 wt% and 2.0 wt% ZnO nanoparticles were separately incorporated into the $CA_4$ biopolymeric hydrogels using the same procedure, as shown in Table 2. The ZnO concentrations (0.5, 1.0, and 2.0 wt%) were calculated based on the total weight of the synthesized polymer hydrogel matrix. The samples were named $CA_4Z_1$, $CA_4Z_2$, and $CA_4Z_3$ based on the composition of the $CA_4$ hydrogel matrix and the ZnO nanoparticles. Here, $CA_4$ represents the base hydrogel formulation (0.040 + 0.025 + 0.025 mol), Z indicates ZnO nanoparticles, whereas the numbers 1, 2, and 3 correspond to 0.5 wt%, 1.0 wt%, and 2.0 wt% ZnO nanoparticles, respectively.

## 2.2. Characterization

### 2.2.1. Fourier Transform Infrared (FT IR) Spectroscopic Analysis

The molecular structure of the $CA_4$-ZnO nanocomposite was characterized using a Shimadzu 8400S FT IR spectrophotometer. Samples were prepared using the standard KBr pellet method, and the spectra were recorded over the range of 4000–500$cm^{-1}$.

**Table 2:** Formulation of CA-TEA-FA in distinct composition after adding ZnO Nanocomposite (wt%).

| S. No | Sample | CA4 Hydrogel Composition (moles) | ZnO Nanocomposite (wt %) | Description of Hydrogels |
|---|---|---|---|---|
| 1 | CA4Z1 | 0.040 + 0.025 + 0.025 | 0.5 | Transparent in nature; brown, glassy gel; insoluble in water |
| 2 | CA4Z2 | 0.040 + 0.025 + 0.025 | 1.0 | |
| 3 | CA4Z3 | 0.040 + 0.025 + 0.025 | 2.0 | |

#### 2.2.2. UV–Vis Spectrophotometry

An ultraviolet–visible double-beam (UV–Vis) spectrophotometer was used to characterize the $CA_4$-ZnO nanocomposite. Samples of the compound were collected periodically to monitor the completion of the reaction. The sample spectra were recorded over a wavelength range of 190–1100 nm.

#### 2.2.3. Scanning Electron Microscopy–Energy-Dispersive X-ray Spectroscopy (SEM -EDX)

To evaluate the effects of polymer and cross-linker concentrations on the surface morphology, the $CA_4$-ZnO hydrogel was characterized using scanning electron microscopy (SEM). SEM coupled with energy-dispersive X-ray spectroscopy (EDX) enabled rapid and accurate qualitative and quantitative analysis of the elemental composition, providing valuable insights into the hydrogel structure.

#### 2.2.4. High-Resolution Transmission Electron Microscopy (HR-TEM)

High-resolution transmission electron microscopy (HR-TEM), operated at 200–300 kV, was used to obtain high-resolution images and structural information at the nanoscale.

#### 2.2.5. Thermogravimetric Analysis (TGA)

The thermal properties of the polymeric hydrogels were investigated using simultaneous thermogravimetric analysis (TGA) with an SDT Q600 (TA Instruments). The TGA curves were recorded over a temperature range from room temperature to 500 °C.

#### 2.2.6. Swelling Behavior

A 0.200 g sample of dried hydrogel was immersed in buffer solutions with pH values ranging from 2.0 to 11.0 at room temperature. At regular time intervals, the swollen hydrogels were carefully removed from the swelling medium, gently blotted with filter paper to remove excess surface water, weighed, and then returned to the original swelling medium. This procedure ensured the accurate determination of the water absorption capacity. Finally, excess surface water was removed from the hydrogels with filter paper. The swelling percentage was calculated using Equation (1):

$$S_{eq}\% = \frac{W_{sq} - W_I}{W_I} \times 100 \quad (1)$$

where, $W_I$ is the initial weight of the dried hydrogel and $W_{Sq}$ is the weight of the swollen sample at equilibrium.

### 2.3. Biological Applications

#### 2.3.1. Antibacterial Studies

The antibacterial activity was evaluated using the conventional agar well diffusion method. Each bacterial isolate was cultured in brain heart infusion (BHI) broth and diluted to approximately $10^5$ colony-forming units (CFU)/mL. The bacterial suspensions were flood-inoculated onto the surface of Mueller–Hinton agar and allowed to dry. Sterile cork borers were used to create wells with a diameter of 5 mm in the agar medium. Subsequently, 30 µL of the sample solution (50 µg compound dissolved in 500 µL DMSO) was placed in each well. The plates were incubated at 37 °C for 18 h. Antimicrobial activity was evaluated by measuring the diameter of the inhibition zone. Dimethyl sulfoxide (DMSO) was used as the solvent control, while ciprofloxacin was used as the standard antibacterial agent. The tests were performed in triplicate. The hydrogels were tested against Staphylococcus aureus, Bacillus subtilis, *Klebsiella pneumoniae*, and *Escherichia coli*.

#### 2.3.2. Antifungal Studies

The antifungal activity was evaluated against *C. albicans* and *A. niger*. Clotrimazole (20 mg/well) was used as the standard. The diameter of the inhibition zone (mm) was used as an indicator of activity against the test pathogens.

#### 2.3.3. Cytotoxic Studies

The mouse fibroblast cell line (L929) was seeded in a 96-well plate at a concentration of $1 \times 10^4$ cells/well in Dulbecco's Modified Eagle Medium (DMEM) supplemented with 10% fetal bovine serum and 1× antibiotic–antimycotic solution. The cells were incubated in a $CO_2$ incubator maintained at 37 °C with 5% $CO_2$. After washing with 200 µL of 1× phosphate-buffered saline (PBS), the cells were cultured for 24 h in serum-free medium containing different concentrations of the test sample, with 25% DMSO used as the positive control. At the end of the treatment period, the culture medium was aspirated from the cells. MTT solution [0.5 mg/mL of (3-(4,5-dimethylthiazol-2-yl)-2,5-diphenyltetrazolium bromide)] prepared in 1X PBS was added, and the cells were incubated for 4 h at 37 °C in a $CO_2$ incubator. After the incubation period, the medium containing MTT was discarded, and the cells were rinsed with 200 µL of PBS. The formed crystals were dissolved in 100 µL of DMSO and mixed

2026, Vol. 1, Article ID. 2026.0003
https://doi.org/10.69709/ESM.2026.109909

thoroughly. The formation of purple-blue formazan dye was quantified by measuring the absorbance at 570 nm using a microplate reader.

#### 2.3.4. Antioxidant Studies

Blois's (1958) method was used to measure the sample's DPPH (2,2-diphenyl-1-picrylhydrazyl) radical-scavenging activity. A 0.5 mL aliquot of the sample solution in methanol was mixed with 2.5 mL of a 0.5 mM methanolic DPPH solution. The reaction mixture was shaken well and kept in the dark at room temperature for 30 min. The absorbance was measured at 517 nm using a UV spectrophotometer. Ascorbic acid was used as the positive control. The percentage of DPPH free radical scavenging activity was determined using the standard formula.

$$\% \text{ of Inhibition} = (\text{Absorbance of control} - \text{Absorbance of sample}/\text{Absorbance of control}) \times 100.$$

#### 2.3.5. Computational Studies

A preliminary computational study was conducted to investigate the antibacterial activity and protein-binding properties of $CA_4$ hydrogels and ZnO nanoparticle-incorporated hydrogels. Therefore, the $CA_4$-ZnO nanocomposite hydrogels were subjected to molecular docking studies.

## 3. Results and Discussion

### 3.1. Spectral Characterization

#### 3.1.1. FT IR Spectroscopy of $CA_4$-ZnO Nanocomposite Hydrogels

A stretching frequency observed at 3360 $cm^{-1}$ corresponds to the hydrogen-bonded O-H stretching vibration [19,20]. The decrease in the stretching frequency from 3414 $cm^{-1}$ to 3360 $cm^{-1}$ may be attributed to the incorporation of ZnO nanoparticles into the polymer network. The peak at 2982 $cm^{-1}$ represents the C-H stretching vibration. A distinct sharp peak at 1732 $cm^{-1}$ is ascribed to C=O stretching [21]. New absorption peaks at 1610 $cm^{-1}$ and 1474 $cm^{-1}$ were attributed to $COO^-$ stretching vibrations. The prominent spectral peak at 1294 $cm^{-1}$ is due to the presence of C-N stretching vibrations found in triethanolamine. The C-O stretching vibration was observed at 1176 $cm^{-1}$ in the polyester network. The peaks at 1073 $cm^{-1}$ and 1041 $cm^{-1}$ were attributed to C-O-C stretching vibrations. The spectral peak appeared at 670 $cm^{-1,}$ confirming the incorporation of zinc oxide nanoparticles into the main chain of hydrogels, as shown in Figure 1 [22].

#### 3.1.2. UV Spectroscopy of [$CA_4$-ZnO] Nanocomposite Hydrogels

UV–Vis spectroscopy is a key analytical technique used to characterize citric acid-, 2-furoic acid-, and triethanolamine-based hydrogels incorporated with zinc oxide (ZnO) nanoparticles. This method helps confirm the incorporation of ZnO nanoparticles into the hydrogel matrix. Figure 2 shows the UV–Vis spectral findings of $CA_4$-ZnO nanocomposite hydrogels. ZnO nanoparticles absorb UV–Vis light over the wavelength range of 250–800 nm [23]. The UV-Visible spectrum of the $CA_4$-ZnO nanocomposite revealed a broad absorption peak at 300 nm, corresponding to an absorbance value of 0.1. The absorbance of a nanocomposite hydrogel is caused by $n \rightarrow \pi^*$ transitions. The λmax primarily corresponds to chromophores containing carbonyl groups. This transition involves the promotion of an electron from a nonbonding (n) orbital, specifically a lone pair on a heteroatom such as oxygen, to an antibonding ($\pi^*$) orbital.

#### 3.1.3. SEM and EDX Analysis of $CA_4$-ZnO Nanocomposite Hydrogels

The surface morphology of the synthesized $CA_4$-ZnO nanocomposite hydrogel was examined using the $CA_4Z_3$ sample by scanning electron microscopy (SEM). The SEM image (Figure 3) reveals a heterogeneous, non-porous surface morphology with a rough structure attributed to the hydrogel matrix containing ZnO nanoparticles, which are irregularly distributed throughout the network. The interaction between the hydrogel polymer chains and ZnO nanoparticles enhances the swelling ability and functional properties of the hydrogel.

To validate the synthesis of the $CA_4$-ZnO nanocomposite hydrogel $CA_4Z_3$, EDX analysis was performed, and the resulting peaks are shown in Figure 4. The EDX analysis confirmed the presence of ZnO nanoparticles in the synthesized nanocomposite. The elemental composition of the nanocomposite, expressed in weight percentage, revealed the presence of carbon (C), oxygen (O), nitrogen (N), and zinc (Zn) at 56.16%, 30.69%, 3.29%, and 7.51%, respectively. The plot of CA4-ZnO nanocomposite hydrogels shows the presence of carbon, nitrogen, oxygen, and zinc (Table 3).

2026, Vol. 1, Article ID. 2026.0003
https://doi.org/10.69709/ESM.2026.109909

SCIFINITI PUBLISHING

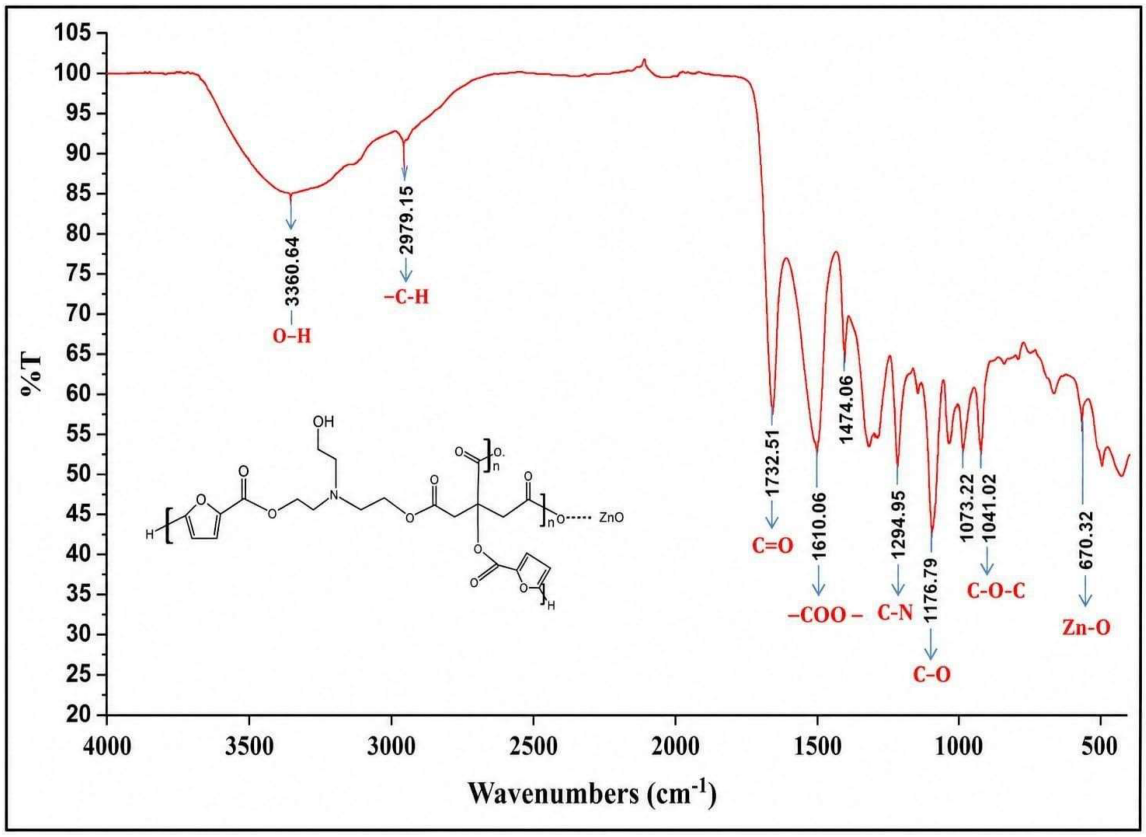



**Figure 1:** FT IR spectrum of $CA_4$-ZnO nanocomposite hydrogels.

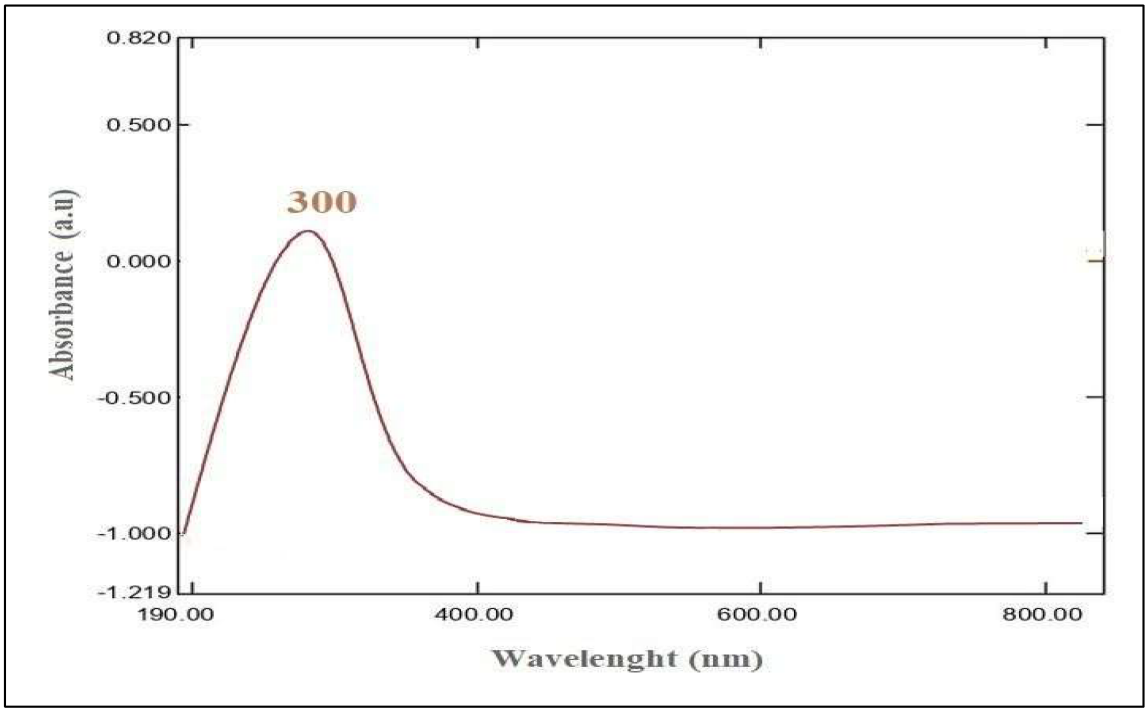



**Figure 2:** UV–Vis spectrum of $CA_4$-ZnO nanocomposite hydrogels.

2026, Vol. 1, Article ID. 2026.0003
https://doi.org/10.69709/ESM.2026.109909

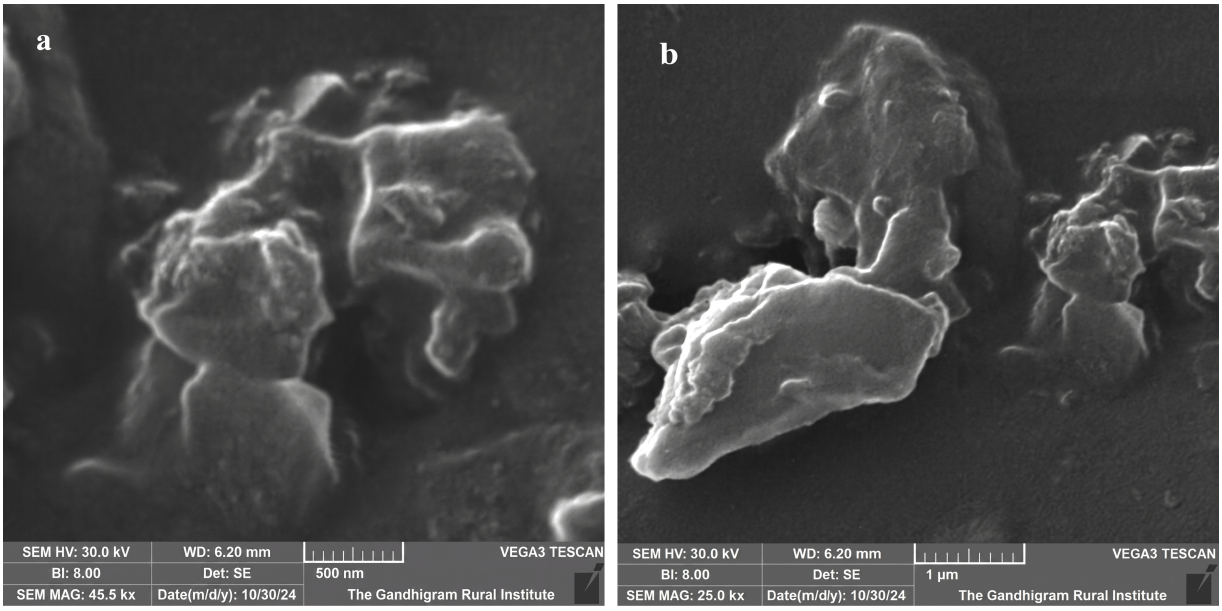



**Figure 3:** SEM analysis of [CA4-ZnO] nanocomposite hydrogels of $CA_4Z_3$.

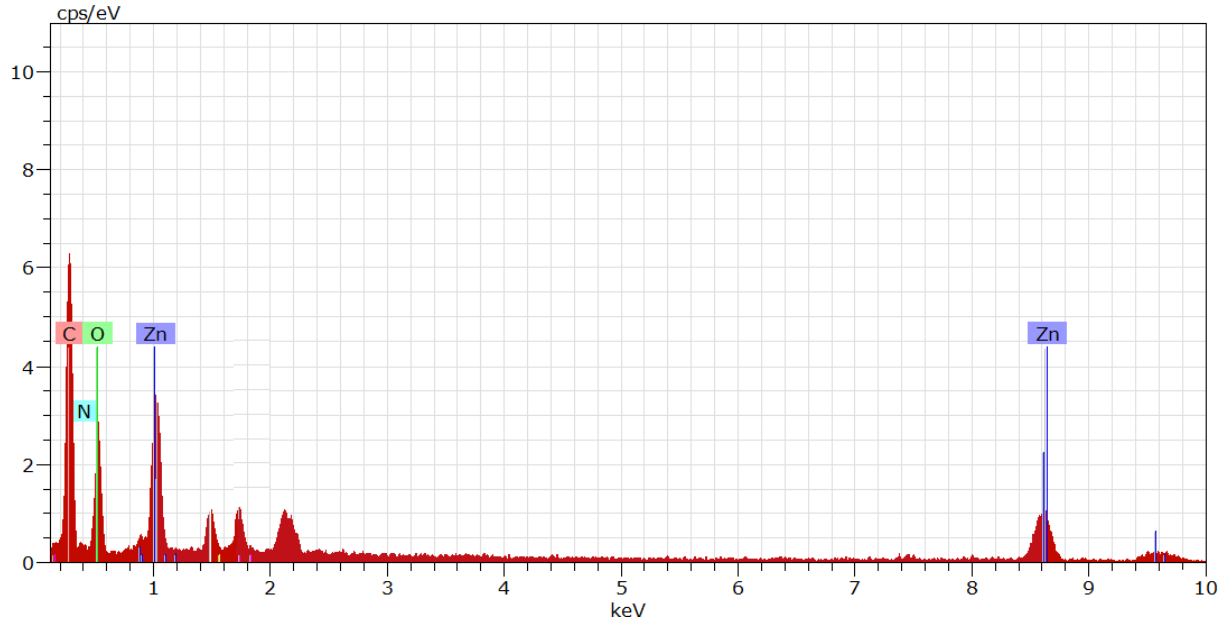



**Figure 4:** EDX analysis of [$CA_4$-ZnO] nanocomposite hydrogels of $CA_4Z_3$.

**Table 3:** Weight percentages of elements in the $CA_4Z_3$ nanocomposite hydrogel.

| S. No | Elements | Atomic number | Weight percentage |
|---|---|---|---|
| 1 | Carbon | 6 | 56.16 |
| 2 | Oxygen | 8 | 30.69 |
| 3 | Nitrogen | 7 | 3.29 |
| 4 | Zinc | 30 | 7.51 |

2026, Vol. 1, Article ID. 2026.0003
https://doi.org/10.69709/ESM.2026.109909



### 3.1.4. HR-TEM Analysis of $CA_4$-ZnO Nanocomposite Hydrogels

The size and structure of nanoparticles within the hydrogel network were examined using transmission electron microscopy (TEM). The TEM images showed that the spherical ZnO nanoparticles were uniformly distributed within the $CA_4$-ZnO hydrogel matrix. The average particle size of the $CA_4$-ZnO nanocomposite was approximately 38 nm (Figure 5). The well-defined spherical morphology of the ZnO nanoparticles indicates strong interactions between the hydrogel matrix and ZnO nanoparticles. Furthermore, the presence of lower concentrations of spherical ZnO nanoparticles enhanced the biological activity, as evidenced by the antibacterial studies [24].

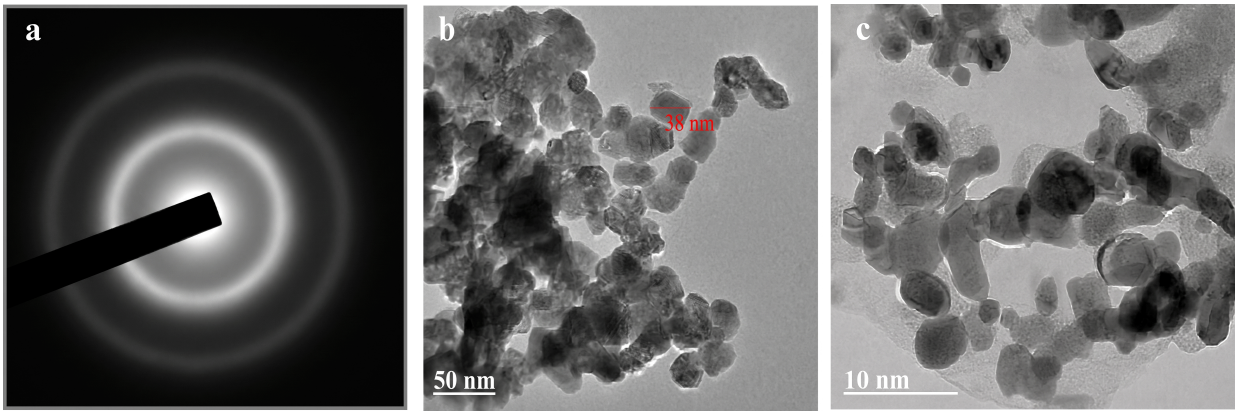



**Figure 5:** HR-TEM analysis of $CA_4$-ZnO nanocomposite hydrogels.

### 3.1.5. TGA of [$CA_4$-ZnO] Nanocomposite Hydrogels

Thermogravimetric analysis (TGA) was performed to investigate the thermal stability of the $CA_4$-ZnO nanocomposite hydrogel, as shown in Figure 6. The TGA curve shows three stages of degradation. The initial stage of degradation occurred between 50 °C and 100 °C, resulting in a 9% weight loss due to the removal of residual water. The second stage of degradation occurred between 150 °C and 250 °C, resulting in a 23% weight loss due to the decomposition of 2-furoic acid substituents from the hydrogel matrix (Figure 6). The third stage of degradation was observed at 300 °C, resulting in a 16% weight loss due to the decomposition of the polymer network containing embedded ZnO nanoparticles [25]. Overall, the TGA study revealed that the ZnO nanocomposite hydrogel exhibited considerable thermal stability, with several degradation stages involving water loss and polymer decomposition. In general, ZnO nanoparticles exhibit high thermal stability under normal conditions. However, their stability can be affected by factors such as impurities, interactions with other materials, and exposure to high temperatures, which may lead to structural degradation. In the present study, the interaction between the biopolymeric hydrogel matrix and ZnO nanoparticles resulted in reduced thermal stability, likely due to polymeric filler interactions [26].

### 3.1.6. Swelling Equilibrium (%) of $CA_4$-ZnO Nanocomposite Hydrogels

ZnO nanoparticles at concentrations of 0.5%, 1.0%, and 2.0%, designated as $CA_4Z_1$, $CA_4Z_2$, and $CA_4Z_3$, respectively, were incorporated into $CA_4$ hydrogels. The swelling behavior of the $CA_4$-ZnO nanocomposite hydrogels at various pH values (2.0, 4.0, 7.0, 9.0, and 11.0) was evaluated, and the results are presented in Table 4. The hydrogels exhibited pH-dependent swelling, with maximal swelling observed under neutral to slightly alkaline conditions (pH 7–9), owing to the ionization of functional groups such as -COOH and -OH in the polymeric matrix, which increases electrostatic repulsion and favors higher water uptake. $CA_4Z_3$ had the largest swelling percentage (127% at pH 7), followed by $CA_4Z_2$ (121%) and $CA_4Z_1$ (117%), as shown in Figure 7. Increasing the concentration of ZnO nanoparticles appears to enhance the swelling capacity, which may be attributed to their interactions with the hydrophilic functional groups within the hydrogel network. At acidic pH (2–4), the swelling ratios decreased due to protonation of functional groups, which promoted hydrogen bonding and network contraction. At a higher alkaline pH of 11, swelling was partially reduced due to charge shielding and partial degradation of the hydrogel network [27]. Overall, the swelling investigation demonstrates that the incorporation of ZnO nanoparticles into

2026, Vol. 1, Article ID. 2026.0003
https://doi.org/10.69709/ESM.2026.109909

the hydrogel is advantageous for applications in drug delivery, wound dressing, and biomedical systems requiring controlled release under physiological pH conditions [28]. The biological activities in the present study were evaluated using $CA_4Z_3$ nanocomposite hydrogels due to their favorable swelling behavior.

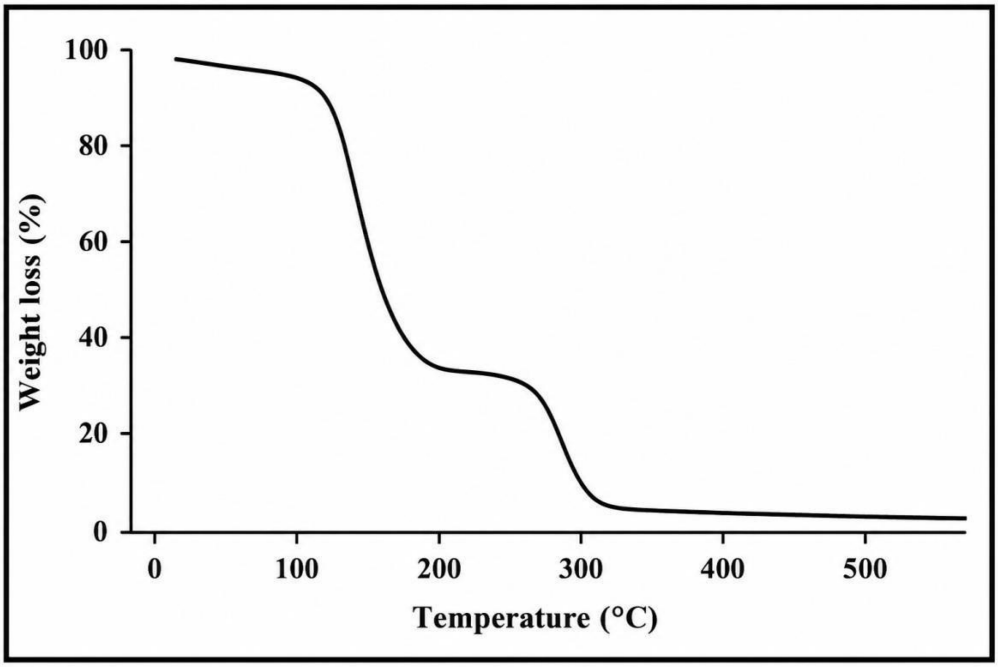



**Figure 6:** TGA of [$CA_4$-ZnO] nanocomposite hydrogels.

**Table 4:** Swelling equilibrium (%) of $CA_4$-ZnO at different pH values.

| S. No | Sample | $CA_4$ Synthesized Hydrogel (in Grams) | ZnO Nano Particles (wt%) | Swelling Equilibrium (%) pH | | | | |
|---|---|---|---|---|---|---|---|---|
| | | | | 2 | 4 | 7 | 9.0 | 11 |
| 1 | CA4Z1 | 0.200 | 0. 5 | 100 | 107 | 118 | 104 | 100 |
| 2 | CA4Z2 | 0.200 | 1.0 | 108 | 113 | 120 | 115 | 107 |
| 3 | CA4Z3 | 0.200 | 2.0 | 112 | 117 | 127 | 121 | 117 |

## 3.2. Biological Activity of [$CA_4$-ZnO] Nanocomposite Hydrogels

### 3.2.1. Antibacterial Activity

$CA_4Z_3$ outperformed all other [$CA_4$-ZnO] hydrogel compositions in terms of antibacterial performance, as shown in Figure 8. The antibacterial activity was evaluated against Gram-positive bacterial strains (*S. aureus and B. subtilis*) and Gram-negative bacterial strains (*E. coli and K. pneumoniae*), using ciprofloxacin as the standard reference drug. The standard drug ciprofloxacin produced inhibition zones of 25 mm against *S. aureus*, 18 mm against *B. subtilis*, 20 mm against *K. pneumoniae*, and 30 mm against *E. coli*. The $CA_4Z_3$ hydrogels exhibited inhibition zones of 0 mm against E. coli, 8 mm against S. aureus, 10 mm against B. subtilis, and 6 mm against *K. pneumoniae* (Figure 8). These findings indicate that the hydrogel exhibited moderate inhibitory activity against *S. aureus, B. subtilis*, and *K. pneumoniae*, whereas *E. coli* showed no antibacterial activity, which may be attributed to variations in cell membrane permeability toward the antibacterial agent [29]. The obtained results demonstrate that $CA_4Z_3$ hydrogels exhibited moderate inhibitory effects, indicating their potential for biological applications.

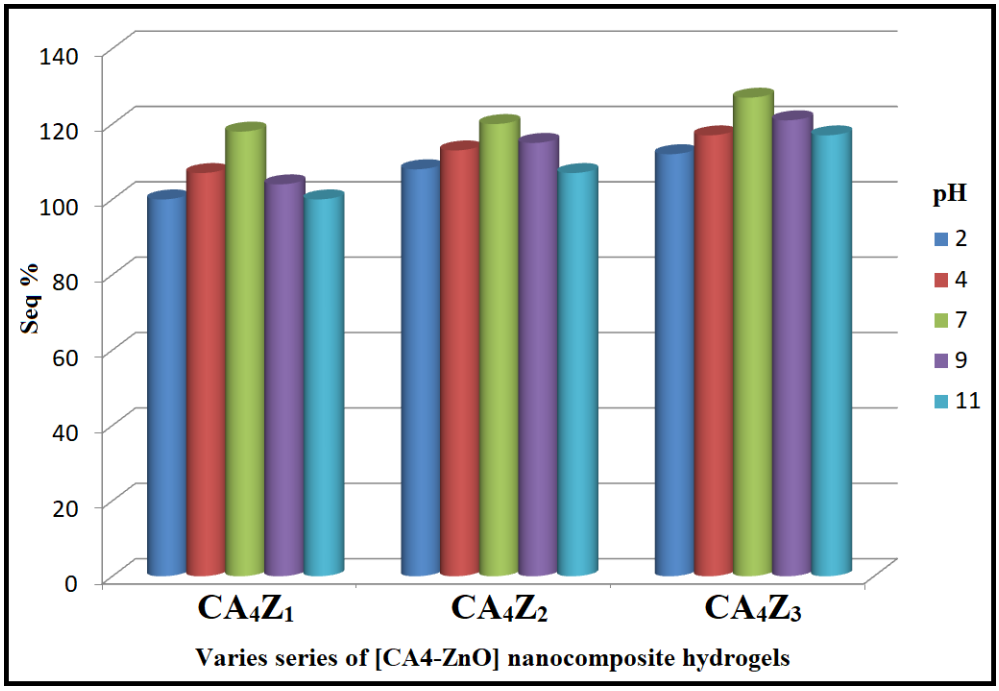



**Figure 7:** Graphical representation of swelling equilibrium (%) of $CA_4$-ZnO at different pH values.

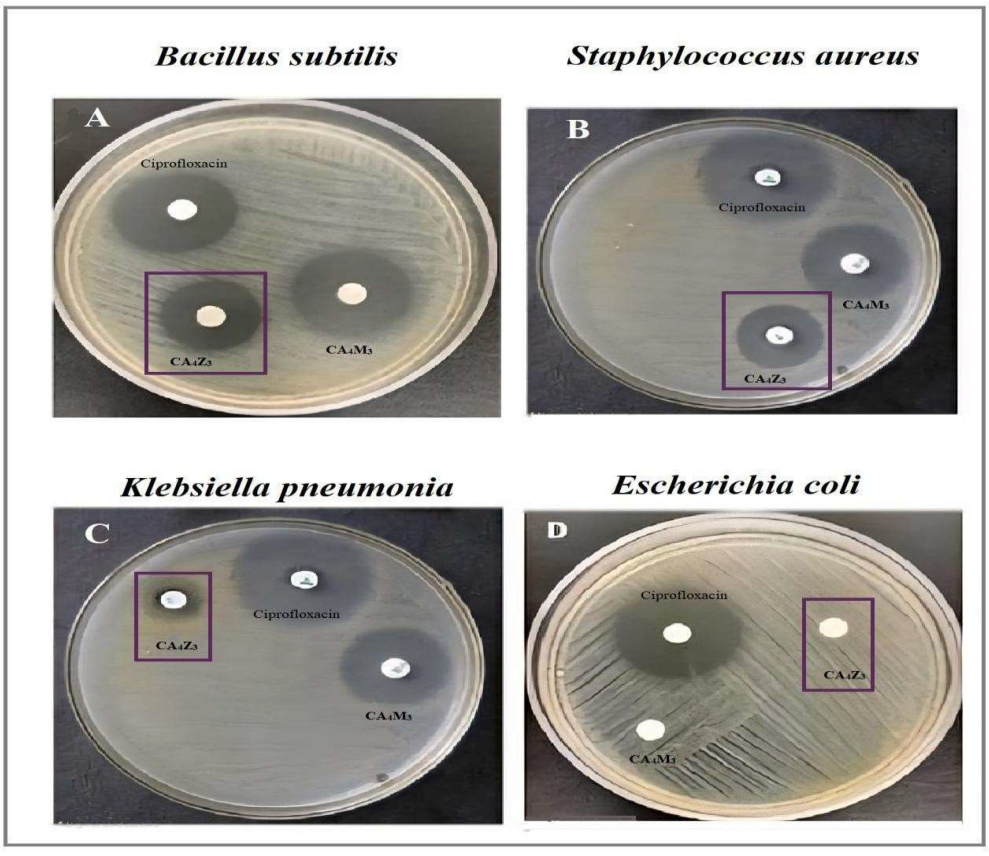



**Figure 8:** Antibacterial activity of $CA_4Z_3$ nanocomposite hydrogels.

2026, Vol. 1, Article ID. 2026.0003
https://doi.org/10.69709/ESM.2026.109909

### 3.2.2. Antifungal Activity

The hydrogels were evaluated for antifungal activity against fungal strains, including *Candida albicans* and *Aspergillus niger*, using the agar well diffusion method. The standard antifungal drug clotrimazole exhibited inhibition zones of 16 mm against *Candida albicans* and 26 mm against *Aspergillus niger*. In comparison, the $CA_4Z_3$ hydrogel at a concentration of 300 mg/well produced a 4 mm inhibition zone against *Candida albicans*, while no inhibition (0 mm) was observed against *Aspergillus niger* (Figure 9). These findings revealed that the antifungal activity of the hydrogel was significantly lower than that of the standard drug. The limited inhibition may be attributed to the robust chitinous cell walls and melanin pigments present in these fungi, which enhance resistance to oxidative stress and reduce the susceptibility of the cells to ZnO nanoparticle attack [30]. Nevertheless, the incorporation of ZnO nanoparticles into polymeric hydrogel matrices may provide a synergistic antifungal platform with potential applications in biomedical and agricultural fields.

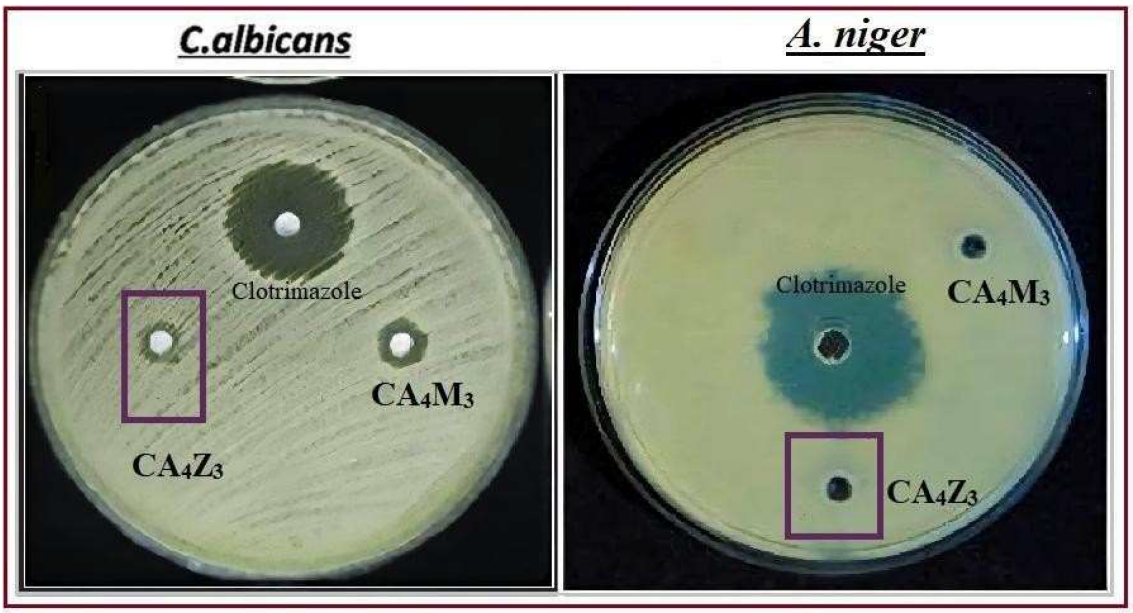



**Figure 9:** Antifungal activity of $CA_4Z_3$ nanocomposite hydrogels.

### 3.2.3. Cytotoxicity Activity

Several studies have investigated the cytotoxicity of ZnO nanoparticles using the MTT assay, demonstrating their effects on a wide range of animal cell types [31]. Figure 10 shows the cell viability% of $CA_4Z_3$ nanocomposite hydrogels. The concentrations of 25, 50, 100, 250, and 500 µg/mL yielded percentages of 95, 90, 90, 85, and 82%, respectively. $CA_4Z_3$ was classified as non-toxic according to the criteria defined by ISO 10993-5 [32]. The average cell viability was greater than 80% at all concentrations. As the result, among the $CA_4$-ZnO nanocomposite hydrogels, $CA_4Z_3$ exhibited a higher percentage of cell viability, particularly at lower concentrations (25, 50, and 100 µg/mL), indicating its suitability and safety for biomedical applications (Figure 11).

### 3.2.4. Antioxidant Activity

The antioxidant activity of $CA_4Z_3$ nanocomposite hydrogels was evaluated using the DPPH radical-scavenging assay, with ascorbic acid as the reference standard. The inhibition rates ranged from 32% to 94% at different concentrations (25, 50, 100, 250, and 500 µg/mL), with corresponding values of 32%, 42%, 67%, 90%, and 94%, respectively. $CA_4Z_3$ hydrogels exhibited antioxidant activity of 42%, 53%, 61%, 68%, and 79% at concentrations of 25, 50, 100, 250, and 500 µg/mL, respectively, as shown in Figure 12.

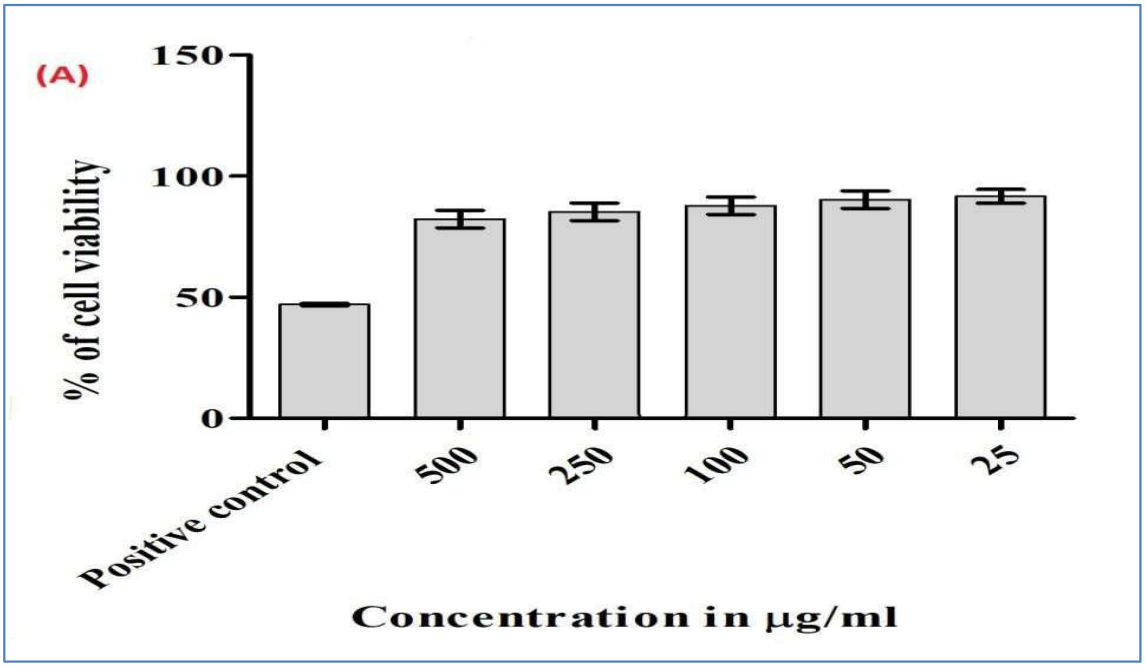



**Figure 10:** MTT Assay of $CA_4Z_3$ at different concentrations.

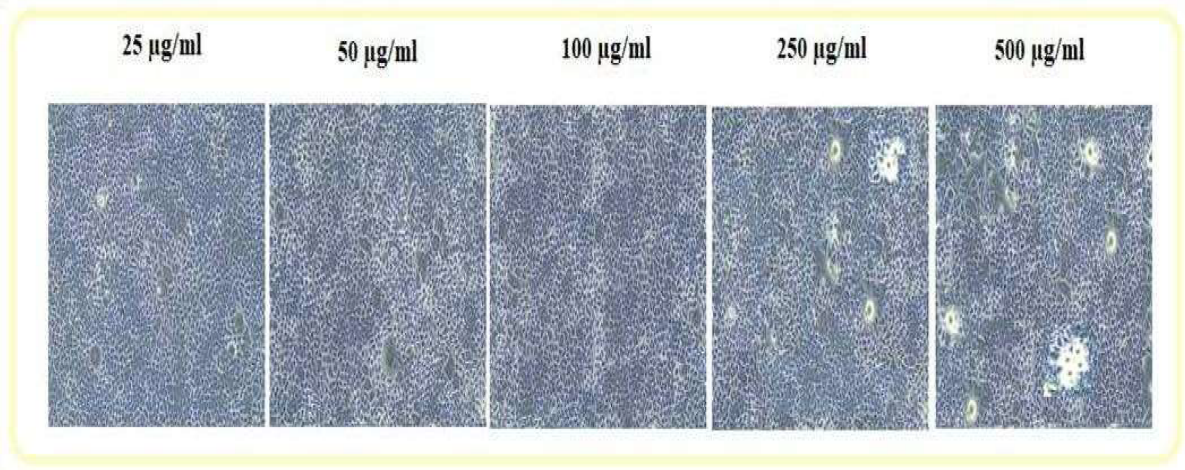



**Figure 11:** The cytotoxicity MTT assay of $CA_4Z_3$ at various concentrations.

At lower concentrations (25 and 50 µg/mL), $CA_4Z_3$ exhibited moderate inhibition, whereas ascorbic acid showed comparatively lower inhibition. At medium concentrations (100–250 µg/mL), the antioxidant activity of $CA_4Z_3$ gradually increased, followed by a further increase in activity at higher concentrations. At the maximum concentration (500 µg/mL), $CA_4Z_3$ exhibited good inhibition compared with ascorbic acid. These results suggest that the ZnO nanocomposite hydrogel possesses significant antioxidant properties, which may be attributed to the interaction of ZnO nanoparticles with free radicals. This may promote electron donation and hydrogen transfer to DPPH radicals through the hydrophilic functional groups (-OH, -NH, and -COOH) present in the hydrogel matrix. The interaction between ZnO nanoparticles and the polymeric network facilitates enhanced radical-scavenging efficacy. The $IC_{50}$ of $CA_4Z_3$ was 149 µg/mL for the DPPH method. The scavenging activity and $IC_{50}$ value exhibit an inverse relationship [33]. Similar findings have also been reported by Patel et al. (2011) [34].

2026, Vol. 1, Article ID. 2026.0003
https://doi.org/10.69709/ESM.2026.109909

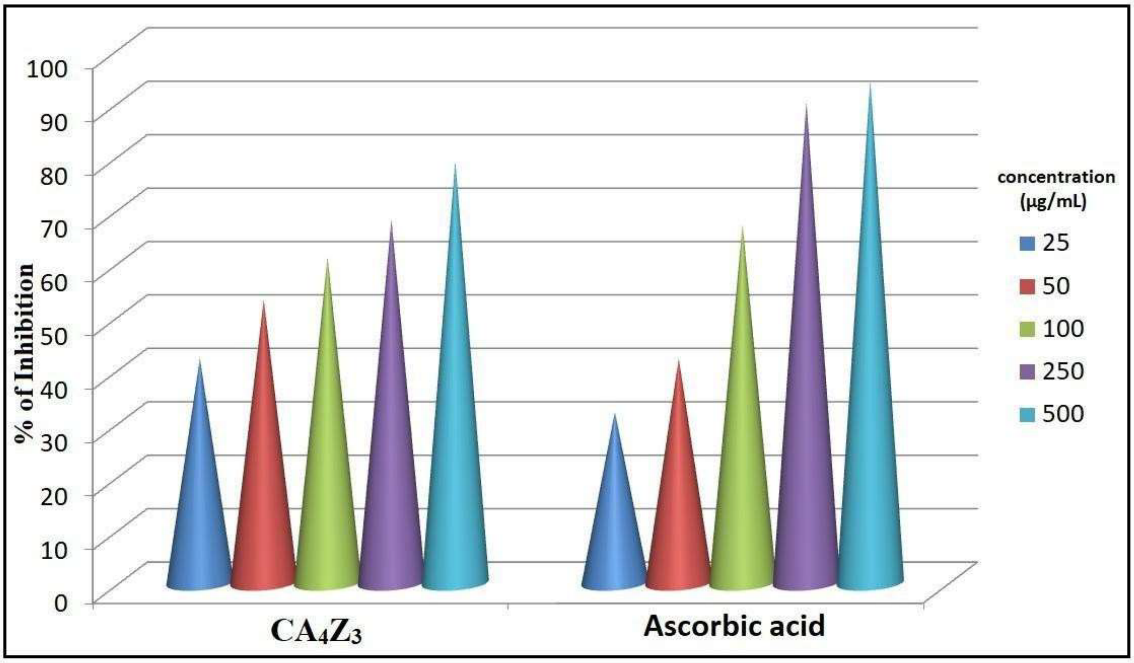



**Figure 12:** Antioxidant activity of $CA_4Z_3$ at distinct concentrations.

## 3.3. Computational Studies of $CA_4$-ZnO Nanocomposite Hydrogels

### 3.3.1. Density Functional Theory (DFT)

Since the $CA_4$-ZnO nanocomposite hydrogels exhibited biological activity, DFT and molecular docking studies were conducted to explore their mechanism of action. Initially, an intrinsic reaction coordinate (IRC) analysis was performed using the three basic monomers, namely citric acid, triethanolamine, and 2-furoic acid, which were utilized in the synthesis of the hydrogels. The IRC study revealed the structure selected for optimization at the DFT level. The monomers were further optimized at the 6-31G(d) level using the B3LYP (Becke, 3-parameter, Lee–Yang–Parr) functional, and the FMOs (Frontier Molecular Orbitals) were visualized to evaluate the molecular orbital (MO) aspects of reactivity. After geometry optimization, the molecular electrostatic potential (MESP) was generated to identify probable reactive regions of the molecule. The optimized molecules were subsequently used for docking studies. The DFT-derived values for the $CA_4$-ZnO nanocomposite hydrogels are presented in Table 5.

**Table 5:** The values generated from DFT calculations of $CA_4$-ZnO nanocomposite hydrogels.

| Description | HOMO eV | LUMO eV | Band Gap eV | Energy H | Dipole D | Symmetry |
|---|---|---|---|---|---|---|
| $CA_4$-ZnO | −6.171 | −2.086 | 4.085 | −3740.41 | 7.8291 | C1 |

The FMO analysis revealed that, although the three monomers combine to form the hydrogel network, the IRC results indicated that the FMOs were unevenly distributed across the individual monomers. After optimization, it was observed that the HOMO (Highest Occupied Molecular Orbital) was primarily localized on the triethanolamine moiety of the hydrogel, whereas the LUMO (Lowest Unoccupied Molecular Orbital) was distributed slightly over the citric acid moiety, in close proximity to the ZnO nanoparticles within the hydrogel network (Figure 13). The 2-furoic acid moiety exhibited no lobes over its structure, indicating the absence of significant reactive regions within this segment. The denser lobes observed near the ZnO nanoparticle region suggest the presence of prominent reactive regions around its center. The MESP illustrates the distribution of electrostatic potential across the molecular surface, including the presence of positive potential regions, as shown in Figures 14 and 15.

These findings suggest that the corresponding moiety contributes to the desired biological activity through electronic effects arising from the coexistence of negative and positive potential regions. A higher-potential region was observed near the ZnO nanoparticle region, and the biological activity was enhanced through the incorporation of ZnO nanoparticles into the hydrogel matrix.

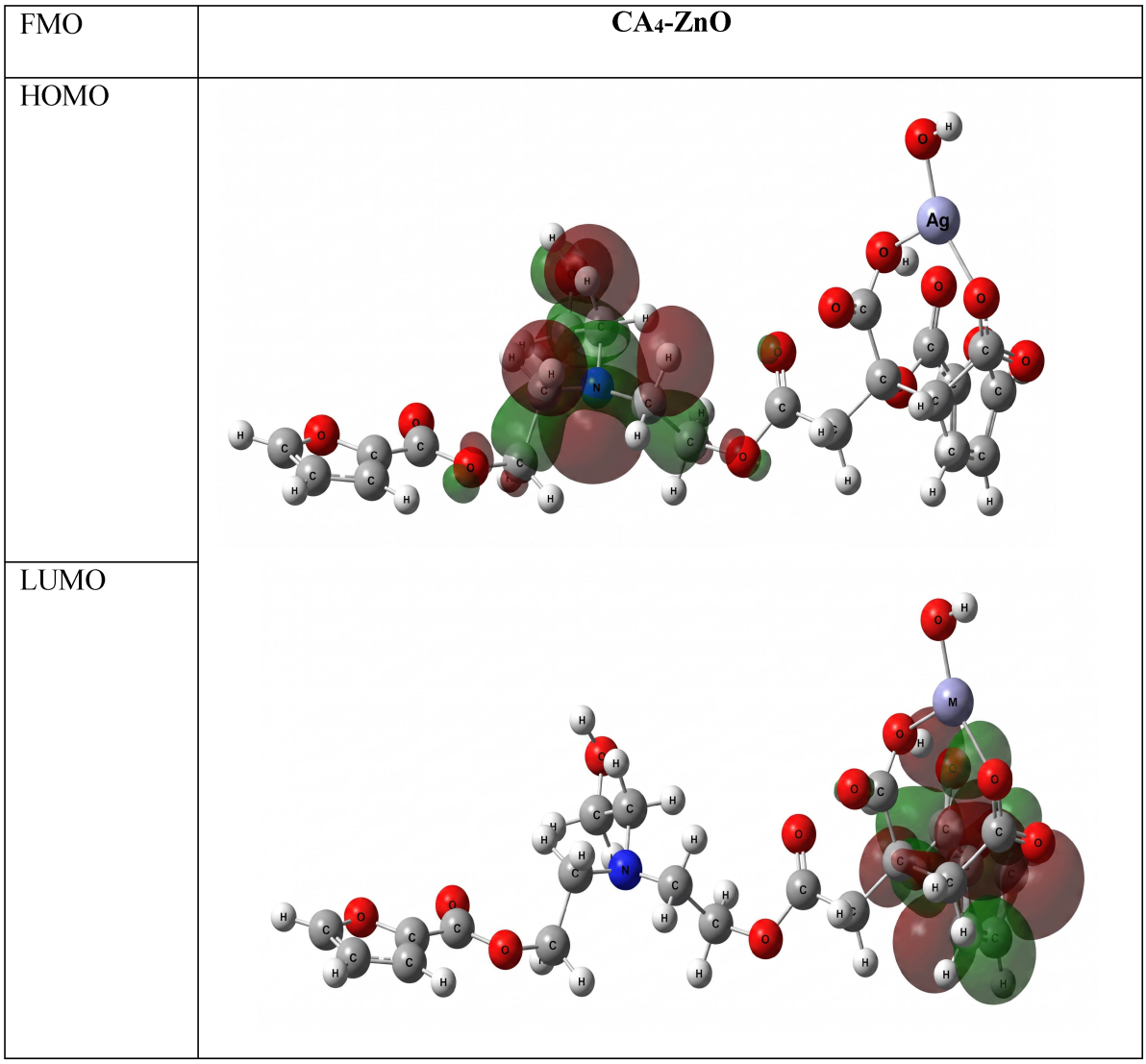



**Figure 13:** Frontier molecular orbital (FMO) and intrinsic reaction coordinate (IRC) of the $CA_4$-ZnO nanocomposite hydrogel.

### 3.3.2. Molecular Docking (PDB ID: 1N67 and 4DXD)

In view of their biomedical properties, the nanocomposite hydrogels were subjected to docking studies against important receptors associated with antibacterial activity and wound healing, including the FtsZ (filamenting temperature-sensitive mutant Z) protein complex [35] and the Staphylococcus aureus protein target Clumping Factor A [36]. Infections caused by drug-resistant strains of Klebsiella pneumoniae represent a major challenge to the efficacy of conventional antibiotics. Therefore, there is an increasing need to investigate alternative antimicrobial therapies, particularly hydrogels synthesized from simple monomeric compounds [37]. Considering the biological importance of hydrogel derivatives, the present study aimed to synthesize, characterize, and investigate the biological potential of the hydrogel using a simple, convenient, and eco-friendly synthetic methodology.

2026, Vol. 1, Article ID. 2026.0003
https://doi.org/10.69709/ESM.2026.109909

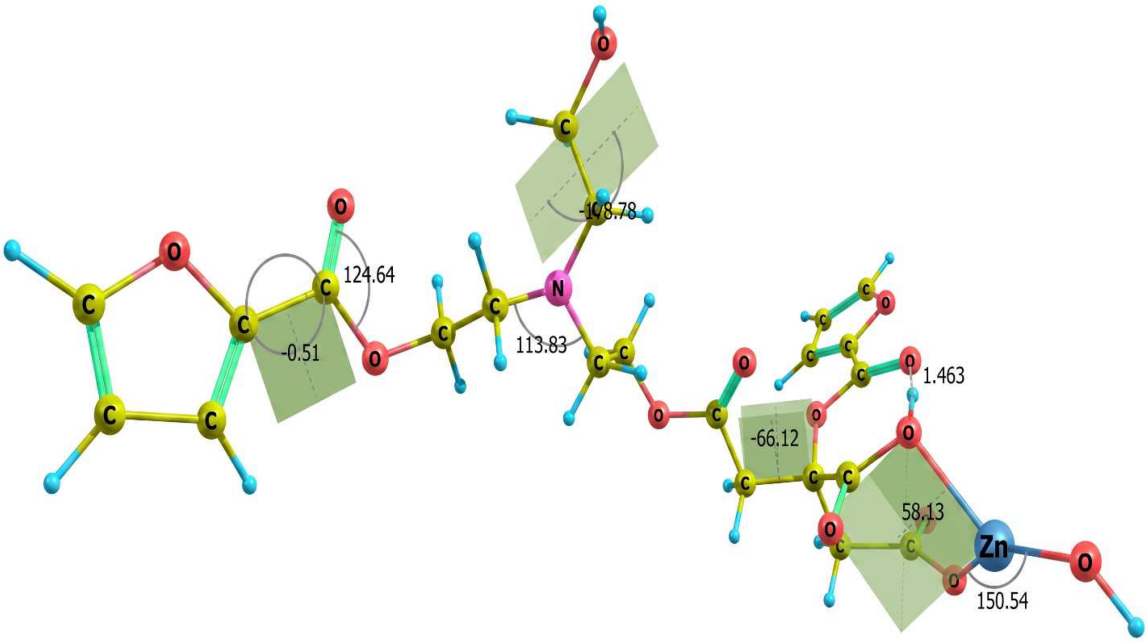



**Figure 14:** The optimized geometry of the $CA_4$-ZnO nanocomposite hydrogels.

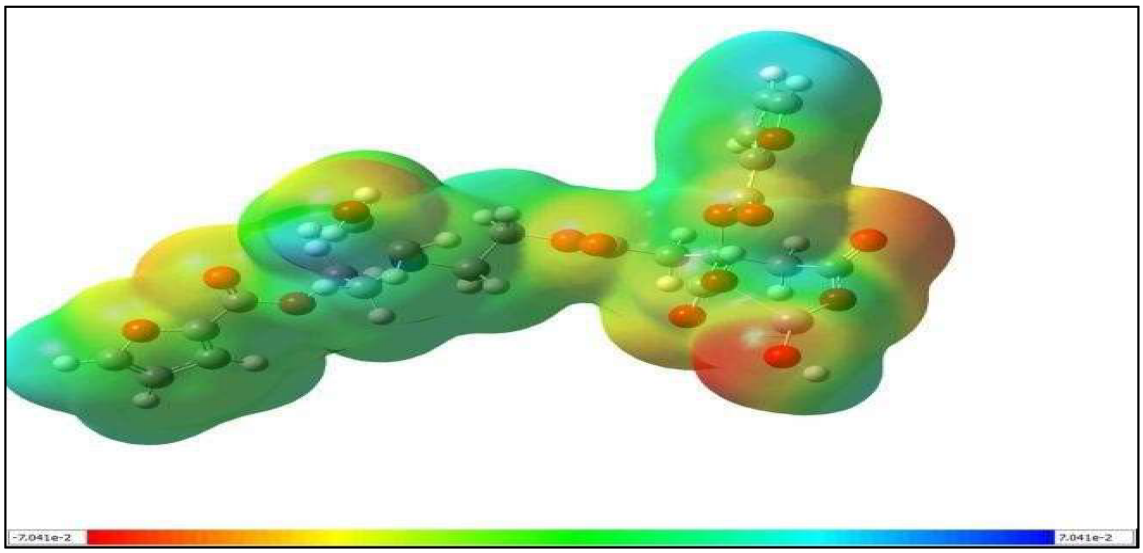



**Figure 15:** The MESP of the $CA_4$-ZnO nanocomposite hydrogels.

The molecular docking study was conducted to evaluate the interactions between $CA_4$-ZnO nanocomposite hydrogels and the FtsZ protein complex (PDB ID: 4DXD), given their strong antibacterial properties. Additionally, $CA_4$-ZnO nanocomposite hydrogels were evaluated against the *Staphylococcus aureus* protein *Clumping Factor A* (PDB ID: 1N67), which demonstrated significant antibacterial activity. Both nanocomposite hydrogels exhibited favorable docking scores. However, the $CA_4$-ZnO nanocomposite hydrogel demonstrated stronger and more favorable binding interactions with the Clumping Factor A protein, as shown in Table 6. The $CA_4$-ZnO nanocomposite hydrogel also demonstrated superior ligand efficiency across all evaluated parameters, including standard ligand efficiency (−0.188), surface area-adjusted ligand efficiency (−0.633), and log-normalized ligand efficiency (−1.543).

**Table 6:** Docking properties of $CA_4$-ZnO nanocomposite hydrogels against Clumping Factor A.

| Property | Clumping Factor a From Staphylococcus Aureus (1N67) $CA_4$-ZnO |
|---|---|
| Docking Score | −7.154 |
| Glide Ligand Efficiency | −0.188 |
| Glide Ligand Efficiency SA | −0.633 |
| Glide Ligand Efficiency LN | −1.543 |
| Glide G Score | −7.154 |
| Glide Evdw | −21.263 |
| Glide Ecoul | −21.754 |
| Glide Emodel | −42.555 |
| Glide Energy | −43.017 |
| Extra Precision (XP) | −7.154 |
| XP HBond | −1.860 |

In the $CA_4$-ZnO–Clumping Factor A complex, the ligand is tightly anchored via hydrogen bonds with polar residues (ASN267, SER268, and GLN235) and stabilized by hydrophobic contacts (VAL270, VAL323, ALA269, and ILE232) and potential electrostatic interactions with ASP273. Water-mediated interactions and minimal solvent exposure further enhance binding stability. These findings suggest that $CA_4$-ZnO nanocomposite hydrogels may serve as effective modulators of *S. aureus* proteins.

### 3.3.3. ADMET (Absorption, Distribution, Metabolism, Excretion, and Toxicity)

The water solubility of a compound (LogS) represents the solubility of the compound at 25 °C. Drugs with higher water solubility are absorbed more efficiently than lipid-soluble compounds, and the obtained value of −2.99 indicates favorable aqueous solubility. Similarly, intestinal absorption predicts the percentage of an orally administered drug that is absorbed. The low absorption value observed in this study suggests that the compound may be more effectively administered through alternative routes rather than oral delivery.

The blood-brain barrier (BBB) indicates the ability of a drug to penetrate the brain and represents an important factor in minimizing side effects and toxicity while enhancing therapeutic efficacy. The evaluated nanocomposite hydrogels were predicted to cross the BBB, as presented in Table 7. The obtained value suggests favorable BBB permeability for the investigated drug delivery system.

**Table 7:** ADMET properties of $CA_4$-ZnO nanocomposite hydrogels.

| Properties | CA4-ZnO |
|---|---|
| Molecular Weight | 592.82 |
| Water Solub | −2.99 |
| Caco2 perm | −0.23 |
| Intest Abs | 32.4 |
| Skin Perm | −2.73 |
| Glycopro substrate | Yes |
| BBB Perm | −2.43 |
| CNS Perm | −3.85 |
| CYP1A inhibitor | No |
| Log P | 0.624 |
| Surface area | 223.12 |

2026, Vol. 1, Article ID. 2026.0003
https://doi.org/10.69709/ESM.2026.109909

## 4. Conclusions

In the current research, pH-responsive $CA_4$ hydrogels with varying nano-ZnO concentrations were developed. The UV analysis of the $CA_4$-ZnO nanocomposite hydrogel revealed a strong peak at 300 nm, indicating the presence of ZnO nanoparticles. FT IR spectroscopy revealed peaks at 1073 $cm^{-1}$ and 1041 $cm^{-1}$, corresponding to the C-O-C stretching vibrations. The peak observed at 670 $cm^{-1}$ confirmed the incorporation of zinc oxide nanoparticles into the hydrogel network. The SEM-EDX analysis of [$CA_4$-ZnO] revealed a heterogeneous, nonporous, and rough surface structure resulting from the incorporation of ZnO nanoparticles within the hydrogel matrix. The ZnO nanoparticles were irregularly distributed throughout the matrix. The EDX spectrum confirmed the presence of carbon (C), oxygen (O), nitrogen (N), and zinc (Zn), with corresponding weight percentages of 56.16%, 30.69%, 3.29%, and 7.51%, respectively. The TEM analysis of [$CA_4$-ZnO] nanocomposite hydrogels revealed a nanoparticle size of approximately 38 nm. The TGA study demonstrated that the ZnO nanocomposite hydrogel exhibited considerable thermal stability, with multiple degradation stages involving water loss and polymer decomposition. The swelling behavior of the hydrogel was also evaluated at varying pH values (2.0–11.0), and the results showed that the swelling capacity and swelling equilibrium were higher under neutral conditions (pH 7). The swelling studies clearly demonstrated that citric acid has the ability to modulate the swelling behavior of the hydrogel. The increased concentration of nano-ZnO in $CA_4Z_3$ resulted in a higher swelling ratio than that of the other hydrogel formulations. Antibacterial investigation of [$CA_4$-ZnO] nanocomposite hydrogels showed moderate inhibitory activity against *S. aureus*, *B. subtilis*, and *K. pneumoniae*, whereas no antibacterial activity was observed against *E. coli*, possibly because of differences in cell membrane permeability toward the antibacterial agent. Similarly, the antifungal assay showed low inhibition, which may be attributed to the presence of robust chitinous cell walls and melanin pigments in *Aspergillus niger* and *Candida albicans*. These structural features provide resistance against oxidative stress and ZnO nanoparticle-mediated activity. The antioxidant activity results demonstrated that $CA_4Z_3$ hydrogels exhibited significant antioxidant properties, particularly at higher concentrations of 100, 250, and 500 μg/mL. The average cell viability in the cytotoxic assays was greater than 80% at all concentrations, indicating potential suitability for biomedical applications. The docking studies revealed that the nanocomposite hydrogels could serve as effective modulators of S. aureus proteins and demonstrated the potential to readily cross the blood-brain barrier (BBB). Overall, the study concludes that the developed biocompatible, pH-sensitive hydrogels have promising applications in industrial and biomedical fields, including tissue engineering, wound healing, drug delivery, and other high-performance biomedical applications.

## List of Abbreviations

| | |
|---|---|
| ADMET | Absorption, Distribution, Metabolism, Excretion and Toxicity |
| ALA269 | Alanine at Position 269 |
| ASN267 | Asparagine at Position 267 |
| ASP273 | Aspartic Acid at Position 273 |
| BBB | Blood-Brain Barrier |
| BHI | Brain Heart Infusion |
| CA | Citric Acid |
| CFU | Colony-Forming Units |
| C NMR | Carbon-13 Nuclear Magnetic Resonance Spectroscopy |
| CT | Citric acid–Triethanolamine |
| CTF | Citric acid–Triethanolamine-2 Furoic Acid |
| DFT | Density Functional Theory |
| DMEM | Dulbecco's Modified Eagle Medium |
| DMSO | Dimethyl Sulfoxide |
| DPPH | 2,2-Diphenyl-1-Picrylhydrazyl |
| EDX | Energy Dispersive X-ray |
| FA | 2-Furoic Acid |
| FMO | Frontier Molecular Orbital |
| FT IR | Fourier Transform Infrared Spectroscopy |
| FtsZ | Filamenting Temperature-Sensitive Mutant Z |
| GLN235 | Glutamine at Position 235 |
| H NMR | Proton Nuclear Magnetic Resonance Spectroscopy |
| HOMO | Highest Occupied Molecular Orbital |
| HR-TEM | High-Resolution Transmission Electron Microscopy |
| ILE232 | Isoleucine at Position 232 |
| IRC | Intrinsic Reaction Coordinate |
| LogS | Logarithmic Value of the Aqueous Solubility of the Compound |
| LUMO | Lowest Unoccupied Molecular Orbital |
| MESP | Molecular Electrostatic Potential |
| MO | Molecular Orbital |
| MTT | 3-(4,5-dimethylthiazol-2-yl)-2,5diphenyltetrazoliumBromide |
| PBS | Phosphate- Buffered Saline |
| PDB | Protein Data Bank |

| | |
|---|---|
| SEM | Scanning Electron Microscopy |
| SER268 | Serine at Position 268 |
| TEA | Triethanolamine |
| TEM | Transmission Electron Microscopy |
| TGA | Thermogravimetric Analysis |
| UV | Ultraviolet Spectroscopy |
| VAL270 | Valine at Position 270 |
| VAL323 | Valine at Position 323 |
| XP | Extra Precision |
| ZnO | Zinc Oxide |

## Author Contributions

Conceptualization and methodology: P.S.R. and G.S.; Investigation and data curation: P.S.R., and G.S.; Formal analysis and validation: G.S.; Software and computational studies (DFT and molecular docking): I.P. and K.A.; Writing—original draft preparation P.S.R.; Writing—review and editing: P.S.R., N.S. and H.S.; Visualization: P.S.R., N.S. and H.S.; Supervision and project administration: G.S. All authors have read and agreed to the published version of the manuscript.

## Availability of Data and Materials

Data supporting the results of this study are available upon request from the corresponding author.

## Conflicts of Interest

The authors declare no conflicts of interest.

## Funding

The study did not receive any external funding and was conducted using only institutional resources.

## Acknowledgments

The authors are grateful to Muthurangam Government Arts College for providing the necessary research facilities to carry out this study.

## AI Declaration

The authors confirm that no part of the scientific content, data analysis, results, interpretations, or conclusions of the manuscript was generated by artificial intelligence (AI). Grammarly and QuillBot were used solely to improve the manuscript's grammar, language quality, sentence structure, and overall readability. The authors reviewed and verified all revisions made by these tools and take full responsibility for the accuracy, integrity, and originality of the manuscript content, in accordance with COPE guidelines and the journal's AI-use policy.

## References

[1] Dodda, J.M.; Deshmukh, K.; Bezuidenhout, D.; Yeh, Y.-C. Hydrogels: Definition, History, Classifications, Formation, Constitutive Characteristics, and Applications. In *Multicomponent Hydrogels*; The Royal Society of Chemistry: London, UK, 2023; pp. 1–25. [CrossRef]

[2] Bashir, S.; Hina, M.; Iqbal, J.; Rajpar, A.H.; Mujtaba, M.A.; Alghamdi, N.A.; Wageh, S.; Ramesh, K.; Ramesh, S. Fundamental Concepts of Hydrogels: Synthesis, Properties, and Their Applications. *Polymers* **2020**, *12*, 2702. [CrossRef] [PubMed]

[3] Dhara (Ganguly), M. Polymer Hydrogels: Classification and Recent Advances. *J. Macromol. Sci. Part A* **2024**, *61*, 265–288. [CrossRef]

[4] Zhang, K.; Liu, Y.; Shi, X.; Zhang, R.; He, Y.; Zhang, H.; Wang, W. Application of Polyvinyl Alcohol/Chitosan Copolymer Hydrogels in Biomedicine: A Review. *Int. J. Biol. Macromol.* **2023**, *242*, 125192. [CrossRef] [PubMed]

[5] De Piano, R.; Caccavo, D.; Barba, A.A.; Lamberti, G. Swelling Behavior of Anionic Hydrogels: Experiments and Modeling. *Gels* **2024**, *10*, 813. [CrossRef] [PubMed]

[6] Zhang, Y.; Wu, B.M. Current Advances in Stimuli-Responsive Hydrogels as Smart Drug Delivery Carriers. *Gels* **2023**, *9*, 838. [CrossRef] [PubMed]

[7] Calderon Moreno, J.M.; Chelu, M.; Popa, M. Biocompatible Stimuli-Sensitive Natural Hydrogels: Recent Advances in Biomedical Applications. *Gels* **2025**, *11*, 993. [CrossRef] [PubMed]

[8] Ren, Z.; Ke, T.; Ling, Q.; Zhao, L.; Gu, H. Rapid Self-Healing and Self-Adhesive Chitosan-Based Hydrogels by Host-Guest Interaction and Dynamic Covalent Bond as Flexible Sensor. *Carbohydr. Polym.* **2021**, *273*, 118533. [CrossRef] [PubMed]

[9] Nicodemus, G.D.; Bryant, S.J. Cell Encapsulation in Biodegradable Hydrogels for Tissue Engineering Applications. *Tissue Eng. Part B Rev.* **2008**, *14*, 149–165. [PubMed]

[10] Chamkouri, H. A Review of Hydrogels, Their Properties and Applications in Medicine. *Am. J. Biomed. Sci. Res.* **2021**, *11*, 485–493. [CrossRef]

[11] Rafael, D.; Melendres, M.M.R.; Andrade, F.; Montero, S.; Martinez-Trucharte, F.; Vilar Hernandez, M.; Durán-Lara, E.F.; Schwartz, S.; Abasolo, I. Thermo-Responsive Hydrogels for Cancer Local Therapy: Challenges and State-of-Art. *Int. J. Pharm.* **2021**, *606*, 120954. [CrossRef] [PubMed]

[12] Danole, A.B.; Kothali, B.K.; Apte, A.K.; Kulkarni, A.A.; Khot, V.S.; Patil, A.A.; Upadhye, S.S. A Review on Hydrogel. *Am. J. PharmTech Res.* **2019**, *9*, 71–81. [CrossRef]

[13] Wang, H.; Du, J.; Mao, Y. Hydrogel-Based Continuum Soft Robots. *Gels* **2025**, *11*, 254. [CrossRef] [PubMed]

[14] Mishra, S.; Rani, P.; Sen, G.; Dey, K.P. Preparation, Properties and Application of Hydrogels: A Review.

In *Hydrogels. Gels Horizons: From Science to Smart Materials*; Springer: Singapore, 2018; pp. 145–173. [CrossRef]

[15] Yadav, A.; Rajhans, K.P.; Ramteke, S.; Sahu, B.L.; Patel, K.S.; Blazhev, B. Contamination of Industrial Waste Water in Central India. *J. Environ. Prot.* **2016**, *7*, 72–81. [CrossRef]

[16] Ghatti, V.; Chapi, S.; Kumar Kumarswamy, Y.; Nandihalli, N.; Kasai, D.R. Strontium-Decorated $Ag_2O$ Nanoparticles Obtained via Green Synthesis/Polyvinyl Alcohol Films for Wound Dressing Applications. *Materials* **2025**, *18*, 3568. [CrossRef] [PubMed]

[17] Pattadakal, S.; Ghatti, V.; Chapi, S.; G., V.; Kumarswamy, Y.K.; Raghu, M.S.; T., V.G.; Nandihalli, N.; Kasai, D.R. Poly(vinyl alcohol) Nanocomposites Reinforced with CuO Nanoparticles Extracted by *Ocimum sanctum*: Evaluation of Wound-Healing Applications. *Polymers* **2025**, *17*, 400. [CrossRef] [PubMed]

[18] Kaushik, M.; Niranjan, R.; Thangam, R.; Madhan, B.; Pandiyarasan, V.; Ramachandran, C.; Oh, D.-H.; Venkatasubbu, G.D. Investigations on the Antimicrobial Activity and Wound Healing Potential of ZnO Nanoparticles. *Appl. Surf. Sci.* **2019**, *479*, 1169–1177. [CrossRef]

[19] Sowmya, R.P.; Harini, S.; Nikila, S.; Guhanathan, S. Investigation on Effect of 3-Trimethoxysilyl Propyl Methacrylate Based Nano-ZnO/CTF Nanocomposite Hydrogel-Synthesis and Characterization. *NanoNEXT* **2025**, *6*, 1–11. [CrossRef]

[20] Sakthivel, M.; Franklin, D.S.; Guhanathan, S. pH-Sensitive Itaconic Acid Based Polymeric Hydrogels for Dye Removal Applications. *Ecotoxicol. Environ. Saf.* **2016**, *134*, 427–432. [CrossRef] [PubMed]

[21] Chitra, G.; Franklin, D.S.; Sudarsan, S.; Sakthivel, M.; Guhanathan, S. Indole-3-Acetic Acid/Diol Based pH-Sensitive Biological Macromolecule for Antibacterial, Antifungal and Antioxidant Applications. *Int. J. Biol. Macromol.* **2017**, *95*, 363–375. [CrossRef] [PubMed]

[22] Helmiyati, H.; Hidayat, Z.S.Z.; Sitanggang, I.F.R.; Liftyawati, D. Antimicrobial Packaging of ZnO–Nps Infused into CMC–PVA Nanocomposite Films Effectively Enhances the Physicochemical Properties. *Polym. Test.* **2021**, *104*, 107412. [CrossRef]

[23] Hamrayev, H.; Shameli, K. Biopolymer-Based Green Synthesis of Zinc Oxide (ZnO) Nanoparticles. *IOP Conf. Ser. Mater. Sci. Eng.* **2021**, *1051*, 012088. [CrossRef]

[24] Mazaheri, N.; Naghsh, N.; Karimi, A.; Salavati, H. In vivo Toxicity Investigation of Magnesium Oxide Nanoparticles in Rat for Environmental and Biomedical Applications. *Iran. J. Biotechnol.* **2019**, *17*, e1543. [CrossRef] [PubMed]

[25] Sheng, L.; Su, L.; Zhang, H. Experimental Determination on Thermal Parameters of Prismatic Lithium Ion Battery Cells. *Int. J. Heat Mass Transf.* **2019**, *139*, 231–239. [CrossRef]

[26] Guhanathan, S.; Devi, M.S.; Murugesan, V. Effect of Coupling Agents on the Mechanical Properties of Fly Ash/Polyester Particulate Composites. *J. Appl. Polym. Sci.* **2001**, *82*, 1755–1760. [CrossRef]

[27] Pourmadadi, M.; Rahmani, E.; Shamsabadipour, A.; Mahtabian, S.; Ahmadi, M.; Rahdar, A.; Díez-Pascual, A.M. Role of Iron Oxide ($Fe_2O_3$) Nanocomposites in Advanced Biomedical Applications: A State-of-the-Art Review. *Nanomaterials* **2022**, *12*, 3873. [CrossRef] [PubMed]

[28] Wang, L.; Riediger, L.; Rao, Q.; Xu, X.; Nie, Y.; Zhou, Y.; Zhang, J.; Tang, P.; Wang, W.; Tacke, F.; et al. Tunable Synthetic Hydrogel Modulates Hepatic Lineage Specification of Human Liver Organoid. *Adv. Funct. Mater.* **2026**, *36*, e08430. [CrossRef]

[29] Leus, I.V.; Zgurskaya, H.I. No Two Are Alike: On the Role of Klebsiella pneumoniae Permeability Barriers in Antibiotic Susceptibility and Persistence. *Antimicrob. Agents Chemother.* **2025**, *69*, e00085-25. [CrossRef] [PubMed]

[30] Azevedo, M.M.; Teixeira-Santos, R.; Silva, A.P.; Cruz, L.; Ricardo, E.; Pina-Vaz, C.; Rodrigues, A.G. The Effect of Antibacterial and Non-Antibacterial Compounds Alone or Associated with Antifugals Upon Fungi. *Front. Microbiol.* **2015**, *6*, 669. [CrossRef] [PubMed]

[31] Nikila, S.; Harini, S.; Sowmya, R.P.; Kubaib, A.; Predhanekar, I.; Guhanathan, S. Synthesis and Computational Assessment of Citric Acid and 1,4-Butanediol Based pH Sensitive Hydrogel Networks for Cationic Dye Adsorption. *Discov. Chem.* **2025**, *2*, 350. [CrossRef]

[32] Hu, Z.; Zhao, R.; Wang, F.; Ren, L.; Wang, L.; Jiang, L. Stimuli-Responsive Hydrogels in Food Sector: Multi-Component Design, Stimulus-Response Mechanisms, and Broad Applications. *Gels* **2026**, *12*, 233. [CrossRef] [PubMed]

[33] Harini, S.; Nikila, S.; Princy Sowmya, R.; Somasundaram, D.; Guhanathan, S. Eco-Friendly Polyester Hydrogel from Almond Gum/Citric Acid/PVA for Efficient Removal of Grenoble Green Dye. *Polym. Renew. Resour.* **2026**, *17*, 104–130. [CrossRef]

[34] Patel, A.M.; Patel, R.G.; Patel, M.P. Super Absorbent Hydrogel Based on Poly [Acrylamide/Maleic Acid/2-Methacryloxy Ethyl Trimethylammonium Chloride]: Synthesis, Characterization and Their Application in the Removal of Chromium (VI) from Aqueous Solution. *J. Macromol. Sci. Part A* **2011**, *48*, 339–347. [CrossRef]

[35] Mustapha, A.; AlSharksi, A.; Eze, U.; Samaila, R.; Ukwah, B.; Anyiam, A.; Samarasinghe, S.; Ibrahim, M. Phytochemical Composition, *In Silico* Molecular Docking Analysis and Antibacterial Activity of *Lawsonia inermis* Linn Leaves Extracts against Extended Spectrum Beta-Lactamases-Producing Strains of *Klebsiella pneumoniae*. *BioMed* **2024**, *4*, 277–292. [CrossRef]

[36] Nguyen, Q.V.; Huynh, D.P.; Park, J.H.; Lee, D.S. Injectable Polymeric Hydrogels for the Delivery of

Therapeutic Agents: A Review. *Eur. Polym. J.* **2015**, *72*, 602–619. [CrossRef]

[37] Ahmed, S.; Rafi, U.M.; Senthil Kumar, R.; Bhat, A.R.; Berredjem, M.; Niranjan, V.; Lavanya, C.; Rahiman, A.K. Theoretical, Antioxidant, Antidiabetic and In Silico Molecular Docking and Pharmacokinetics Studies of Heteroleptic Oxovanadium(IV) Complexes of Thiosemicarbazone Based Ligands and Diclofenac. *J. Biomol. Struct. Dyn.* **2024**, *42*, 8407–8426. [CrossRef]

**Disclaimer/Publisher's Note:** The views expressed in this article are those of the author(s) and do not necessarily reflect the views of the publisher or editors. The publisher and editors assume no responsibility for any injury or damage resulting from the use of information contained herein.